Recent Advances in Antenna Pattern Measurement at Millimetre Wave Frequencies in a Spherical Near-Field Range

Z. Tian, S.F. Gregson, D.G. Gentle

Department of Engineering, Materials and Electrical Science,National Physical Laboratory,Teddington, UK
zhengrong.tian @npl.co.uk

Keywords: millimetre wave, antenna pattern measurement, spherical near-field, scattering suppression

Abstract

This paper presents a distributed millimetre wave spherical near field antenna measurement system for working in the frequency range of 140 GHz to 220 GHz. Both the mechanical and electrical setup are detailed. The mechanical stability of the measurement system during the acquisition has been identified as one of the key factors that affect the measurement accuracy and a good practice is proposed to address the mechanical instability issue for improved measurement accuracy. Room scattering is another major error source. The spherical mathematical absorber reflection suppression (S-MARS) technique was employed for scattering reduction of antenna pattern measurement up to 220 GHz. The effectiveness of scattering reduction using S-MARS was examined and reported.

1 Introduction

Antenna measurement capabilities for frequencies below 110 GHz are well established with calibrations being routinely undertaken at this frequency region in the National Physical Laboratory (NPL) spherical range. The higher millimetre wave frequency bands, for example 140 GHz and 220 GHz, although not widely used in the past, are attracting greater interest and gaining more importance due to the advance of automotive, security and meteorological applications which require short range and broad band radars. To meet the likely demand for antenna calibration at these frequencies, NPL has recently upgraded its spherical near-field range for performing antenna pattern measurements up to 220 GHz. In this paper, the upgrade of the 220 GHz antenna measurement system is described, with both the mechanical and electrical setups detailed. The mechanical stability of the measurement system has been identified as being one of the key factors that affect the measurement accuracy in this frequency region due to the fact that the wavelength is on the order of a few millimetres and any slight movement and instability of the antenna under test (AUT) and the RF subsystem will have a significant impact on the measurement. A good practice is proposed to address the mechanical instability issue for improved measurement accuracy. Range scattering is another significant error source, and the level of range scattering when working at 220 GHz was evaluated. The spherical mathematical absorber reflection suppression measurement and mode filtering technique (S-MARS) [1] was employed in an attempt to reduce the level of room scattering. The acquisition and data processing steps are detailed and preliminary evaluation results are reported.

2 Test system setup

The NPL spherical test range is housed inside a temperature controlled (23 ± 1°C) 15m long by 7.5m wide by 7.5m high fully screened anechoic chamber. The AUT is mounted on a phi-over-theta spherical positioner (Figure 1 (a)) and is most often configured to operate in AUT receive mode. At each theta position, the phi positioner rotates clockwise looking into the AUT which results in the pattern ϕ angle in the antenna coordinate system measured anti-clockwise as illustrated in Figure 1 (b). The transmit antenna, *i.e.* probe, is installed on a polarisation positioner on the transmit tower which sits on a pair of precision linear rails so that the range length, *i.e.* the separation between the transmit antenna and the AUT can be adjusted to the desired optimum distance.

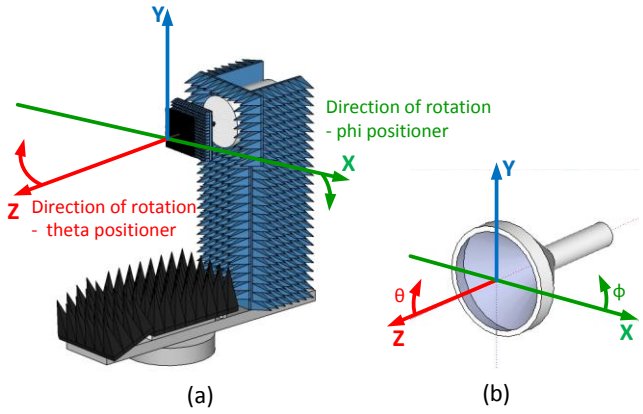

Figure 1: (a) Phi-over-theta positioner stack-up.
(b) Illustration of the antenna coordinate system.

The millimetre wave RF sub-system, as shown in Figure 2, is a PNA-X based distributed system with both the multipliers and mixers located in close proximity to the source antenna and the AUT, so as to minimise losses and maximise the available dynamic range and optimise the link budget. With the exception of the PNA-X, all of the other RF equipment are installed inside the anechoic chamber which isolates both the antenna and measurement devices from outside interference and stray fields. The output signal from the Keysight PSG signal generator was up converted to 140 – 220 GHz through the use of a Virginia Diodes Inc. (VDI) Model WR5.1 Vector

Network Analyser (VNA) Extender Unit. A pair of VDI WR5.1R6 Even Harmonic Mixers (EHM) were used to generate the reference and test IF signals which were fed back to a Keysight 85309A LO/IF distribution unit which was also located within the chamber to manage cable losses.

A lot of considerations and careful planning have been put into how to arrange various RF devices for the purpose of achieving high system stability. In particular, at the transmit end, the source antenna needs to be rotated by 90° for the measurement of two orthogonal electric field components, *i.e.*, E_θ and E_ϕ. It is unavoidable that some changes to the system will be introduced when the source antenna is rotated and this change must be kept to the minimum in order to keep the system stable and minimise the channel imbalance. To achieve this, a bespoke platform was manufactured and bolted to polarisation positioner and the equipment within the dashed line shown in Figure 2 were placed and secured on this platform, and they are rotated together with the source antenna when the polarisation is changed. The feed cable to the up-converter was connected to the PSG through a rotary joint to help reduce variations in the phase and amplitude of the transmitted signal during the polarization change.

After the millimetre wave subsystem was installed, the LO power to the mixers at both the transmit and receive end were set to the optimal value for best achievable system linearity and dynamic range by adjusting the detector voltage on 85309A LO/IF Distribution Unit to the correct level. A power meter was used to monitor the output LO power whilst the detector voltage was adjusted. It is worth noting that when measuring the LO power at one port, the other port should be terminated with a 50Ω load for accurate measurement. It was found necessary to place a 3dB attenuator between the directional coupler and the transmit mixer to achieve the same LO power level to the transmit and to the receive sides. This attenuator also helps to improve the system stability as it dampens any reflected LO from the diplexer and reduces the level of standing waves within the transmit LO cable.

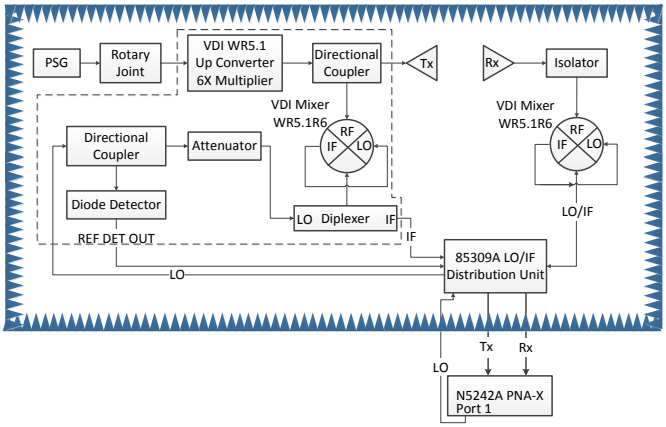

Figure 2: Overview of PNA-X based mm-wave RF subsystem for AUT Rx mode.

The system was found to be very stable with a drift in amplitude measured over a 12 hour period being less than 0.1 dB. The measurement of the AUT was repeated five times over a 10 day period with the AUT disconnected and reconnected into the system and a repeatability of better than 0.13 dB was recorded. During this 10 day period, the range temperature variation was within ±0.1° which again is very encouraging and was sufficiently small that there was no need to resort to return-to-point measurements to compensate for the thermal drift effects.

3 Measurement modes

For the purposes of these tests, the AUT was a circular horn antenna with an aperture diameter of 10 mm. It was polar mounted on the phi-over-theta spherical positioner, with its aperture located over the origin of the measurement coordinate system, *i.e.* at the intersection of the theta and phi axis. The separation between the source antenna and the AUT was 1 metre. The conventional polar mode spherical near-field measurements were taken and the data was transformed to the far-field using standard spherical mode expansion based transformation software.

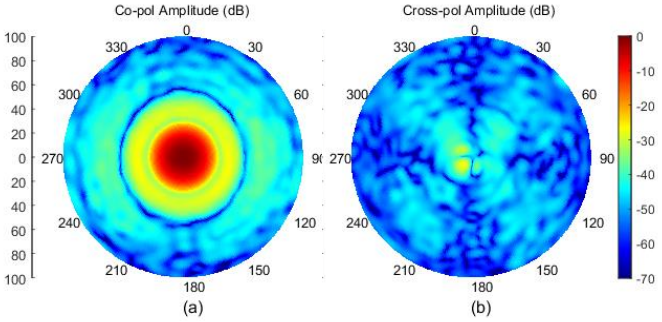

Figure 3: Far-field antenna pattern at 190 GHz using step mode acquisition.

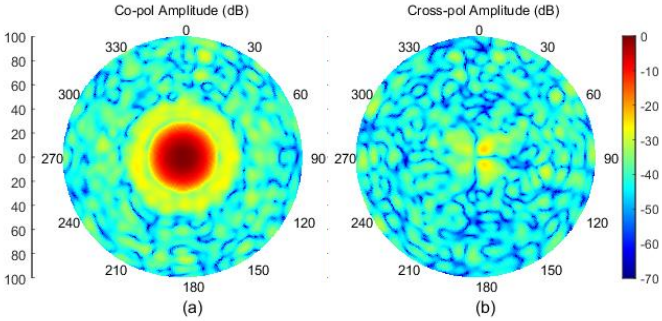

Figure 4: Far-field antenna pattern at 190 GHz using continuous mode acquisition.

During spherical near-field acquisition, the positioner steps in the theta axis with Δθ increment, and scans around the phi axis with Δϕ increment (Figure 1 (a)). The positioner can be operated in two scan modes: step mode or continuous scan mode. In step mode, the positioner stops after rotating to the target position before making the measurement, whilst in continuous mode, the measurement takes place whilst the

positioner is rotating. That is to say, the positioner is not stopped for the RF measurement. When measurement efficiency is of primary concern, continuous mode acquisition is a preferred operational mode and works well at microwave frequencies. However, at millimetre wave frequencies, it is found that measurements using continuous mode acquisition suffers from increased measurement error.

Figure 3 and Figure 4 compare the antenna far-field pattern (pattern plots are presented in true-view coordinate system and resolved onto a Ludwig III polarisation basis and this convention applies to all the pattern plots presented in this paper) measured at 190 GHz using the same angular increment ($\Delta\theta$ and $\Delta\phi$) in step mode and continuous mode, respectively. Strong spurious ripples can be seen in the antenna pattern acquired using continuous mode.

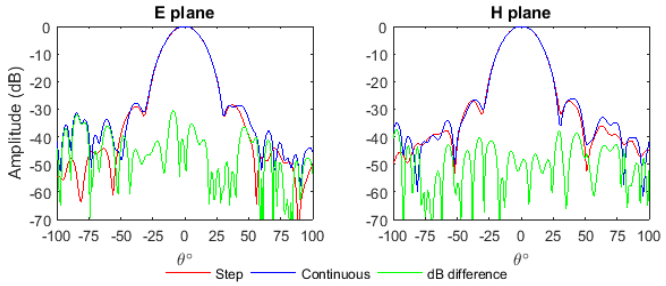

Figure 5: Comparison of far-field E and H plane pattern cuts at 190 GHz using step and continuous mode.

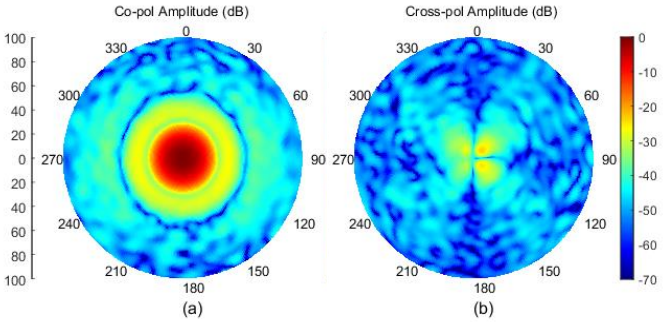

Figure 6: Far-field antenna pattern using continuous mode with oversampling at 190 GHz.

Figure 5 compares the measured boresight E and H plane cuts using the step and continuous mode acquisitions. It can be seen that the worst case error signal introduced by the continuous mode was around 35 dB near boresight. When operating in continuous mode, the AUT and the receive circuitry, including the cables attached to it, are all moving continuously. Any mechanical instability or movement and slight bending of the RF cables *etc*. may cause a measurement error. This indicates that the measurement at such high millimetre wave frequencies is very sensitive to any mechanical instability. This finding suggests it is important to measure in step mode at millimetre wave frequencies if the best measurement accuracy is to be achieved.

If operating in continuous mode, the measurement accuracy can be improved by using oversampling in the near-field acquisition to reduce the noise floor and by limiting the number of spherical modes used within the transform to the same as that used for normal sampling during the spherical transformation process. Figure 6 shows the antenna pattern for the same AUT measured at 190 GHz using continuous mode was improved by using a sampling rate of four times greater than that suggested by the spherical sampling theorem.

4 Room Scattering

Room scattering is typically one of the more significant error sources within the facility level uncertainty budget [2]. This is caused by the imperfect anechoic chamber environment, including any RAM (Radar-Absorbing Material) board located straight behind the AUT and source antenna. Tessellating TeraHertz RAM tiles from Thomas Keating were placed behind both the source antenna and the AUT to help reduce the multiple reflections for antenna measurements in this millimetre wave frequency region. Although multiple reflections can be controlled and reduced to some extent, there is always a certain level of room scattering which exists in the anechoic chamber environment. The measurement and post processing technique, MARS has been found to be an effective technique for identifying and reducing the room scattering through a mathematical approach [3,4]. It is generic and can be applied to planar (P-MARS), cylindrical (C-MARS) and spherical (S-MARS) systems [3,4,5,6,7,8]. In this section, S-MARS is employed for room scattering reduction for the antenna measurement in the NPL spherical near-field range in the frequency range of 140 to 220 GHz.

The MARS technique is well documented in the open literature and so only an overview is presented herein. The key steps involve measurement of the AUT when having deliberately displaced the AUT from the origin, which is in contrast to normal measurement practice where the aperture of the AUT is placed over the intersection of the theta and phi axis. This arrangement enables the higher order mode due to the scattering to be identified and subsequently removed from the transformed pattern results through mode filtering [9].

The field radiated by the AUT into free space can be defined using a spherical wave expansion [1]:

$$\vec{E}(r,\theta,\phi) = \sum_{n=1}^{N}\sum_{m=-n}^{+n}\left[Q_{TEmn}\vec{F}_{TEmn}(r,\theta,\phi) + Q_{TMmn}\vec{F}_{TMmn}(r,\theta,\phi)\right] \quad (1)$$

Where n is the polar index ($1 \le n \le N$), and m is the azimuth index ($-n \le m \le n$) of the spherical modes. N is the upper limit of the truncated mode, and it is determined by r_0, the minimum radius sphere, which is also referred to as the maximum radial extent (MRE) and the frequency. As a rule-of-thumb, N can be determined from the spherical sampling theorem using [10]:

$$N = kr_0 + 10 \quad (2)$$

Where k is the wave factor: $k = \frac{2\pi}{\lambda}$ and r_0 is the MRE of the AUT, which is determined by the size of the AUT and also the relative position of the AUT with respect to the origin of the measurement coordinate system and the term 10 is a safety margin which depends upon the accuracy required.

Q_{TEmn} and Q_{TMmn} are the complex spherical mode expansion coefficients (SMCs) for TE and TM mode respectively. These spherical expansion coefficients are calculated during the spherical near-field to far-field transformation and the amplitude level of these coefficients represents the power distribution in the spherical modes.

$\vec{F}_{TEmn}$ and $\vec{F}_{TMmn}$ are the spherical vector wave function for TE and TM modes, respectively. The form of $\vec{F}_{TEmn}$ and $\vec{F}_{TMmn}$ can be found in [1] and are not detailed here.

As noted in the previous section, the AUT has a diameter of 10 mm. When its aperture is over the origin, its MRE is 5 mm, which gives N = 30. The measured field pattern was transformed to the far-field and its SMCs were calculated. Figure 7 (a) and (e) illustrate the amplitude of the SMCs for TE and TM modes, respectively, with the AUT aperture over the origin.

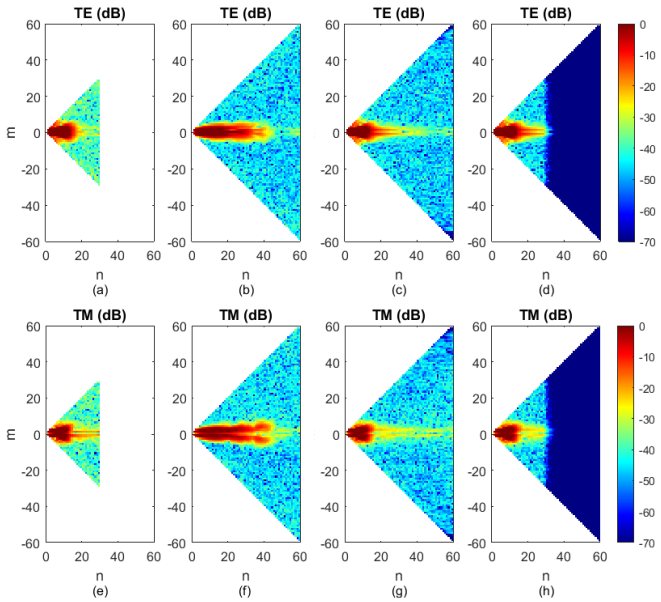

Figure 7: Amplitude (in dB) plots of TE and TM mode SMCs. (a) and (e): AUT over the origin; (b) and (f): AUT displaced by 10 mm; (c) and (g): Displaced AUT moved to the origin through phase change; (d) and (h): mode filters applied.

For the purpose of performing S-MARS processing, the AUT was moved along the Z axis and away from the source antenna by 10 mm. A displacement of 10 mm was chosen so that the offset amount was large enough for S-MARS to capture and identify the higher order modes. This resulted in a larger MRE, and a subsequent larger number of N, which became 60, as shown in Figure 7 (b) and (f). It can be seen that with larger MRE, the energy spread over a larger number of modes. The transformed far-field pattern of the offset AUT is shown in Figure 8.

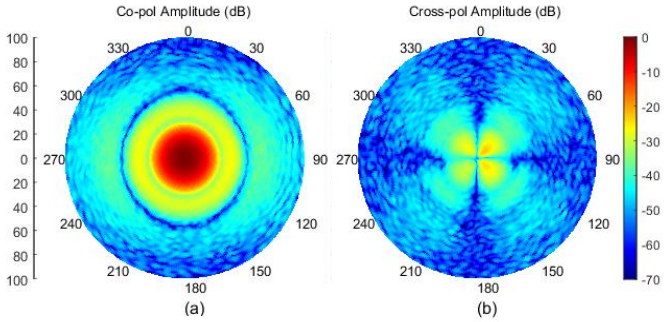

Figure 8: Far-field pattern of the AUT offset from the origin by 10 mm at 190 GHz. (a) co-pol; (b) cross-pol.

The second step in S-MARS processing is to perform a phase change on the transformed electric far-field to mathematically "move" the AUT back to the origin. When the AUT is moved to the origin, the amplitude of E_θ and E_ϕ at the infinite range will not change, however the phase will. The amount of phase change and hence the amount of phase correction that should be applied is:

$$Phase\ Correction = +2\pi * Z_{offset} * \frac{\cos(\theta)}{\lambda} \qquad (3)$$

The SMCs were calculated again after the phase change and its amplitude is presented in Figure 7 (c) and (g). By comparing with the SMCs before phase change, it can be seen that the phase change has taken effect: most of the energy is stored in modes less than 30, very similar to the mode amplitude distribution when the AUT was over the origin. However, the difference between the two scenarios, *i.e.*, the AUT is measured over the origin, and the AUT is displaced and then moved back to the origin mathematically, is that in the second scenario, the amount of multipath reflections "seen" by the AUT were maximised, which can be seen clearly by comparing Figure 8 and Figure 3, and by doing so, and through the phase change, the higher order modes caused by the room scattering were able to be identified and then removed.

After the phase change, the AUT was mathematically moved to the origin and consequently its MRE was decreased to 5 mm. With a MRE of 5 mm, according to Equation (2), only modes which are lower than 30 are necessary for representing the AUT far-field pattern. Conversely, modes with index higher than 30 are primarily due to the multiple reflections which should be filtered and removed. S-MARS filter (Equation (3)) [2] was employed and the filtered SMCs were plotted in Figure 7 (d) and (h).

$$f_n = \begin{cases} 1 & |n| \le N \\ 0.5^{|n|-N} & n > N \end{cases} \qquad (4)$$

Using the filtered SMCs, the far-field pattern of the AUT can be re-constructed and is shown in Figure 9. Here, it can be seen

that the influence of room scattering on the far-field pattern has been significantly reduced by applying S-MARS processing.

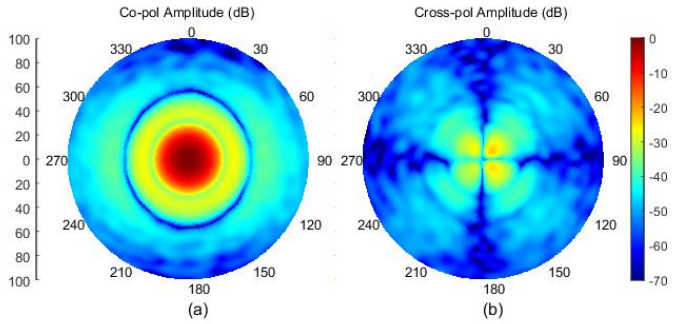

Figure 9: Far-field pattern of the AUT with S-MARS mode filter applied at 190 GHz. (a) co-pol; (b) cross-pol.

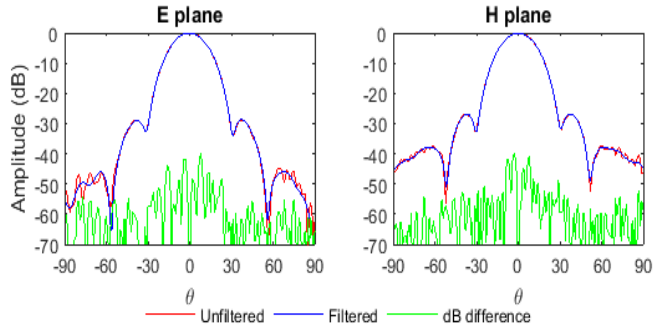

Figure 10: Far-field pattern with and without S-MARS.

Figure 10 compares the far-field *E* and *H* plane pattern cuts of the AUT with and without S-MARS processing. Here, it can be seen that there was far less spurious ripple in the pattern obtained through S-MARS, and the worst case room scattering level near the boresight was around 40 dB at 190 GHz.

5 Conclusions and discussions

The configuration of a distributed millimetre wave spherical near-field antenna test range for working at frequencies from 140 to 220 GHz were detailed. It is identified that at this higher millimetre wave frequency range, the antenna pattern measurement is very sensitive to any mechanical instability of the AUT itself and the receive circuitry attached to it. It is recommended for best measurement accuracy to adopt a step mode acquisition scheme for the antenna pattern measurement.

The S-MARS technique was employed for room scattering reduction and its effectiveness was demonstrated through the measurement at 190 GHz. It was estimated that the room scattering level was around 40 dB. The range was optimised for working at microwave frequencies and typically has a room scattering level of better than 55 dB for below 110 GHz. Further work will look into ways of reducing the multipath reflection at this frequency region. Also a full wave simulation to emulate the actual S-MARS measurement is planned so as to further validate and quantify S-MARS for room scattering reduction at higher millimetre wave frequencies.

Acknowledgements

The authors gratefully acknowledge the funding support provided by the UK National Measurement System and the Department for Business, Energy and Industrial Strategy (BEIS) that enabled the work that this paper presents.

References

[1] C.G. Parini, S.F. Gregson, J. McCormick, D. Janse van Rensburg, "Theory and Practice of Modern Antenna Range Measurements", IET Press, 2014, ISBN 978-1-84919-560-7.

[2] A.C. Newell, "Error Analysis Techniques for Planar Near-field Measurements", *IEEE Transactions on Antennas and Propagation*, vol. AP-36, pp. 754-768, June 1988.

[3] G.E. Hindman, A.C. Newell, "Reflection Suppression in a large spherical near-field range", *AMTA 27th Annual Meeting & Symposium*, Newport, RI, October. 2005.

[4] G.E. Hindman, A.C. Newell, "Reflection Suppression To Improve Anechoic Chamber Performance", *AMTA Europe 2006*, Munch, Germany, March 2006.

[5] S.F. Gregson, A.C. Newell, G.E. Hindman, "Reflection Suppression In Cylindrical Near-Field Antenna Measurement Systems – Cylindrical MARS", *AMTA 31st Annual Meeting & Symposium*, Salt Lake City, UT, November 2009.

[6] S.F. Gregson, A.C. Newell, G.E. Hindman, "Reflection Suppression in Cylindrical Near-Field Measurements of Electrically Small Antennas", *Loughborough Antennas & Propagation Conference*, November, 2009.

[7] S.F. Gregson, A.C. Newell, G.E. Hindman, M.J. Carey, "Extension of the Mathematical Absorber Reflection Suppression Technique to the Planar Near-field Geometry", *AMTA*, Atlanta, GA, October, 2010.

[8] S.F. Gregson, A.C. Newell, G.E. Hindman, P. Pelland, "Range Multipath Reduction in Plane-Polar Near-field Antenna Measurements", *AMTA*, Seattle, October 2012.

[9] O. M. Bucci, G. D'Elia, M. D. Migliore, "A General and Effective Clutter Filtering Strategy in Near-Field Antenna Measurements," *Microwaves, Antennas and Propagation, IEE Proceedings*, vol. 151, no. 3, pp. 227-235, 21 June 2004.

[10] J.E. Hansen, "Spherical near-field antenna measurements", Peter Peregrinus Ltd., London, United Kingdom, 1988.

[11] S.F. Gregson, A.C. Newell, P.N. Betjes, C.G. Parini, "Verification of Spherical Mathematical Absorber Reflection Suppression in a Combination Spherical Near-Field and Compact Antenna Test Range", *AMTA Symposium*, Atlanta Georgia, October, 2017.